Electronic properties and 4*f*→5*d* transitions in Ce-doped Lu_2SiO_5: a theoretical investigation

Lixin Ning,*[a] Lihua Lin,[a] Lanlan Li,[a] Changbao Wu,[a] Chang-kui Duan,[b] Yongfan Zhang,[c] and Luis Seijo*[d,e]

The electronic properties and the 4*f*→5*d* transitions of the dopant Ce^{3+} ions located at the two crystallographic lutetium sites of Lu_2SiO_5 (LSO) are investigated using the hybrid density functional theory (DFT) with the HSE06 functional and the wavefunction-based embedded cluster methods, respectively. The HSE06 calculations give a band gap of 6.35 eV for LSO, which agrees well with the reported experimental values between 6.4–6.8 eV. It is found that Ce^{3+} prefers strongly to occupy the seven-coordinated (Lu1) site over the six-coordinated (Lu2) one. The energy gaps between the occupied Ce^{3+} 4*f* band and the valence band maximum of the host are predicted to be 2.81 and 3.07 eV for Ce_{Lu1} and Ce_{Lu2} substitutions, respectively, which are close to the experimental data of 2.6–2.9 eV. Based on the wavefunction-based CASSCF/CASPT2 embedded cluster calculations for the energies of the Ce^{3+} $4f^1$ and $5d^1$ levels, the experimentally observed 4*f*→5*d* transition bands are identified in association with the two substitutions. The predicted transition energy and intensity patterns for Ce_{Lu1} substitution are in fairly good agreement with those of the experimental absorption spectrum. The variations of the two lowest 4*f*→5*d* transition energies with the substitutions are finally discussed in terms of the changes of the centroid-energy difference and the crystal-field splitting with the local coordination geometries.

[a] *Department of Physics, Anhui Normal University, Wuhu, Anhui 241000, China*
[b] *Department of Physics, University of Science and Technology of China, Hefei, Anhui, 230026, China*
[c] *Department of Chemistry, Fuzhou University, Fuzhou, Fujian 350002, China*
[d] *Departamento De Químca, Universidad Autónoma de Madrid, 28049 Madrid, Spain*
[e] *Instituto Universitario de Ciencia de Materiales Nicolás Cabrera, Universidad Autónoma de Madrid, 28049 Madrid, Spain*

1. Introduction

Cerium-doped optical materials have attracted a great deal of interest due to their wide applications as scintillators, light-emitting diodes, and field emission displays.[1–3] Among these, cerium-doped lutetium oxyorthosilicate, Lu_2SiO_5:Ce (LSO:Ce), has been the subject of considerable attention during the past two decades, because it has a number of appealing properties for scintillator applications in positron emission tomography and other medical imaging equipment.[4,5] It has a relatively high density (7.4 g cm^{-3}), an excellent light yield, a fast scintillation decay time (~40 ns), and the mechanical and chemical stabilities characteristic of oxide structures. The optical properties and luminescence mechanisms of this material have been studied extensively using various experimental methods, including emission, excitation and absorption spectra,[6–10] and thermally stimulated luminescence.[11] It is established that the observed optical spectra mainly come from 4*f*–5*d* electronic transitions of the dopant Ce^{3+}, and oxygen vacancies play a major role in the scintillation afterglow.

However, the identification of the dopant sites associated with the experimentally observed 4*f*→5*d* transition bands in LSO:Ce has been controversial for many years. Suzuki and coworkers[6] observed two distinct types of emission and the correlated excitation spectra of Ce^{3+} in LSO, and these results were explained as due to the existence of two sets of Ce^{3+} centers (referred to as Ce1 and Ce2) occupying the two crystallographically independent lutetium sites. This is known as the two-activation-center model. The emission from Ce2 was observed to be much weaker than that from Ce1, and was obscured by the latter at temperatures above 80 K. Later, Naud et al.[8] gave a different interpretation for the two activation centers, according to which the two types of spectra were from to the Ce^{3+} ions at the substitutional Lu sites and at the interstitial sites, respectively. After that, based upon the 4*f*→5*d* absorption measurements, Cooke and coworkers[9] provided evidence in support of the previously proposed two-activation-center model by Suzuki et al.,[6] but also tentatively suggested that the Ce1 and Ce2 centers were due to the Ce^{3+} ions located at the six-coordinated Lu2 and the seven-coordinated Lu1 sites, respectively. A more recent investigation of LSO:Ce using electron paramagnetic resonance (EPR) spectroscopy indicated that about 95% of the dopant Ce^{3+} ions occupy the Lu1 site, and the rest (about 5%) of Ce^{3+} is at the Lu2 site.[12] These EPR results are in agreement with the two-activation-center model,[6] and attribute the Ce1 and Ce2 centers to the Ce_{Lu1} and Ce_{Lu2} sites, respectively, contrary to the assignment by Cooke et al..[9] Since the information about the location of Ce^{3+} ions in LSO is essential to the understanding of the relevant spectroscopic and scintillation properties, we have performed first-principles calculations to obtain this information in association with the observed $4f \rightarrow 5d$ transitions. Such calculations can provide information on the local geometries around Ce^{3+}, the energy levels involved in $4f$–$5d$ transitions, and also their relationships, as shown in recent works.[13–15]

The energy position of localized Ce^{3+} $4f$ states within the host band gap is an important parameter in many technological applications of Ce-doped optical materials. DFT calculations within the standard local density approximation (LDA) or the general gradient approximation (GGA) are unable to correctly predict this position due to the self-interaction errors associated with the localized $4f$ states.[16–18] One common way to address this problem is to use the so-called DFT+U approach,[19–21] where a Hubbard U correction is applied to the localized $4f$ states while leaving the other electronic states described by the standard DFT. DFT+U can describe properly the energy position of the occupied Ce $4f$ state relative to the top of the valence band by a suitable choice of U, but the band gap underestimation inherent in the exchange-correlation (XC) functionals still remains.[15] Hybrid DFT, where a portion of Hartree-Fock (HF) exchange is mixed with the DFT XC functionals, has been shown to give much better band gaps than the standard DFT, and also better positions of the localized states in oxide systems.[22,23] In addition, admixture of the HF exchange is a universal parameter applied to all the electronic states of the system. It is thus interesting to investigate the electronic properties of the present Ce-doped system using the hybrid DFT method, and to see the improvement in the description of the localized 4f states with respect to the standard DFT.

In the present study, we have first performed geometry optimizations of LSO:Ce using the standard DFT-GGA calculations with the periodic supercell model, in which a cerium atom occupies either of the two lutetium (Lu1 or Lu2) sites. Hybrid DFT calculations have then been carried out on the optimized supercell geometries to investigate their electronic properties. After that, using the optimized supercell structures, we have constructed the Ce_{Lu1}-

or Ce_{Lu2}-centered embedded clusters with their lattice environments represented by *ab initio* model potentials (AIMP), for which the wavefunction-based CASSCF/CASPT2 calculations at the spin-orbit level have been performed to obtain the energies of $4f^1$ and $5d^1$ levels that are involved in the $4f\rightarrow5d$ transitions. By comparing the DFT total energies of Ce_{Lu1}- and Ce_{Lu2}-doped supercells, and also the calculated and experimental $4f\rightarrow5d$ transition energies, the relative preference of the Ce_{Lu1} and Ce_{Lu2} substitutions and their associations with the observed $4f\rightarrow5d$ transition bands have been studied. The main aim of the present work is to use elaborate *ab initio* approaches to gain insight into the identification of the dopant sites in connection with each of the experimentally observed $4f\rightarrow5d$ transition bands in Ce-doped LSO, and to assess the effectiveness of the hybrid DFT in describing the electronic structure of the dopant Ce^{3+}. The remainder of this paper is organized as follows. The methodology and computational details are described in section 2. The results for the structural properties, electronic properties, and the $4f\rightarrow5d$ transition energies are presented and discussed in section 3, with the final conclusions collected in section 4.

2. Methodology

The Ce-doped LSO was modeled using a 1×2×1 supercell containing 128 atoms, in which one of 32 lutetium atoms was substituted by a cerium at Lu1 or Lu2 site (3.125% doping concentration). The atomic coordinates and lattice parameters were fully relaxed without constraints on symmetry or overall spin, by means of periodic DFT[24,25] calculations using the pure PBE XC functional[26,27] and the plane wave basis sets, as implemented the Vienna *ab initio* simulation package (VASP).[28,29] The $4f^{14}5p^65d^16s^2$ electrons on Lu, the $3s^23p^2$ electrons on Si, the $2s^22p^4$ electrons on O, and the $5s^25p^64f^15d^16s^2$ electrons on Ce, were treated as valence electrons. Their interactions with the respective cores were described by the projected augmented wave (PAW) method.[30] The geometry optimizations were performed using the conjugate gradient technique, until the total energies were converged to 10^{-6} eV and the Hellmann-Feynman forces on the atoms were less than 0.01 eV Å^{-1}. With the PBE-optimized geometries, the electronic properties were studied using the hybrid DFT with the HSE06 functional.[31,32] Due to the high computational cost of the hybrid DFT with plane wave basis sets, only single-point energy calculations were performed. In HSE06, 25% of the Fock exchange is mixed with 75% of the PBE exchange, and the slowly decaying long-range part of the Fock exchange is replaced by the corresponding PBE counterpart, with the range separation controlled by a screening parameter (= 0.2 $Å^{-1}$). The HSE06 functional is not free from adjustable parameters, namely, the Fock exchange contribution and the screening length, both of which can be tuned with respect to the experimental results. However, for the purposes of the present study, HSE06 was employed with the default settings. Considering the large size of the supercell, only one *k*-point Γ was used to sample the Brillouin zone, and to achieve converged results, the cutoff energy for the plane wave basis was set to 550 eV.

Based on the geometries of the Ce_{Lu1}- and Ce_{Lu2}-doped LSO supercells as optimized by the standard DFT-PBE calculations, the $4f \rightarrow 5d$ transition energies were computed with the wavefunction-based embedded cluster approaches. The $(Ce_{Lu1}O_7Si_4)^{5+}$ and $(Ce_{Lu2}O_6Si_4)^{7+}$ clusters were chosen for our investigation (see Fig. 1), which comprise the coordination polyhedrons around Ce_{Lu1} and Ce_{Lu2} ions, plus four Si^{4+} ions in the respective second coordination spheres. The total numbers of 693 and 678 ions within the spheres of a radius 10.0 Å surrounding these two clusters were modeled using the AIMP embedding potentials,[33] in order to account for the electrostatic, exchange, and Pauli interactions of the clusters with their environments. The AIMP embedding potentials for Si^{4+} and O^{2-} were taken from those produced in SiO_2,[34] and for Lu^{3+}, the potential for Lu_2O_3 was used.[35] The remainders of their surroundings were simulated by 92607 and 92624 point charges located at lattice sites, respectively, generated using Lepetit's method.[36] This method is an extension of the one proposed by Evjen[37] and produces the same electrostatic potentials as Ewald's method.[38]

For the two embedded clusters, we performed state-average CASSCF (SA-CASSCF)[39–42] plus CASPT2[43–45] calculations with the scalar relativistic many-electron Hamiltonian, which take into account the bonding, static and dynamic correlation effects. Then, with the wavefunctions from SA-CASSCF and energies from CASPT2, the AMFI approximation of the DKH spin-orbit coupling operator[46–48] was added to the Hamiltonian and a restricted active space state-interaction spin-orbit (RASSI-SO) method[49] was employed to account for the spin-orbit effect. These wavefunction-based calculations were performed using the program MOLCAS.[50]

In the SA-CASSCF calculations, a [4*f*, 5*d*, 6*s*] complete active space was adopted. The CASSCF wavefunctions come from interactions of all configurations in which the single unpaired electron occupies one of the thirteen molecular orbitals of main characters Ce^{3+} 4*f*, 5*d*, and 6*s*. The molecular orbitals are optimized by minimizing the average energy of the thirteen states. Since no symmetry (or C_1 symmetry) was found for Ce_{Lu1} or Ce_{Lu2} site in the DFT-PBE geometry optimization, these states may be labeled by the irreducible representation (A) of the C_1 point group, each prefixed by a number i (i=1-13) in order of increasing energy. The states are thus denoted by 1-13^2A, where the superscript "2" indicates the doublet state with spin S = 1/2. With the CASSCF wavefunctions and the occupied and virtual orbitals, CASPT2 calculations were carried out, where dynamic correlation effects of the Ce^{3+} 5s, 5p, 4f and 5d electrons and the O 2s, 2p electrons are considered. Further inclusion of spin-orbit coupling mixes all of these states, leading to thirteen Kramer's doublets that belong to the Γ_2 irreducible representation of the C_1^* double group. In these calculations, a relativistic effective core potential ([Kr] core) with a (14s10p10d8f3g)/[6s5p6d4f1g] Gaussian valence basis set from ref. 51 was used for Ce, and a [He] core effective core potential with a (5s6p1d)/[2s4p1d] valence basis set from ref. 52 was used for O. For Si, we used a [Ne] core effective potential and a (7s6p1d)/(2s3p1d) valence basis set from ref. 52. These basis sets were further augmented by the respective auxiliary spin-orbit basis sets for a proper description of the inner core region in the spin-orbit calculations.

3. Results and discussion

3.1 Structural properties

The structure of the undoped LSO (monoclinic $C2/c$ symmetry) was first optimized using the standard DFT-PBE method, and the results are listed in Tables 1 and 2 for the lattice and internal parameters, respectively. The optimized lattice parameters, which were obtained with the Lu 4f^{14} electrons treated in the core (labeled by Lu-4f core in Table 1), agree very well with the experimental data,[53] while the results with the Lu 4f^{14} electrons treated as valence electrons (labeled by Lu-4f val) are clearly overestimated. Similar observations have been reported in the DFT-PBE calculations of the geometries for the Lu_2O_3 and $LuAlO_3$ crystals,[15,54] traced to the insufficient cancellation of the self-interaction errors associated with the localized Lu 4f electrons in the PBE XC functional. For the two crystallographically different types of lutetium atoms (Lu1 and Lu2), the silicon atom, and the five distinct types of oxygens (O1-O5), which are all located at sites of C_1 symmetry, the calculated internal parameters in the Lu 4*f*-core and Lu 4*f*-val schemes are both in good agreements with the experimental data,[53] see Table 2. In light of these results, the Lu 4*f*-core scheme has been employed in the following geometry optimizations for the Ce-doped LSO.

Table 3 summarizes the calculated lattice parameters for the Ce_{Lu1}- and Ce_{Lu2}-doped LSO supercells, along with those of the undoped LSO for comparison. From the table, we see that the substitution of a Ce into the Lu1 or Lu2 site produces a very small increase (by 0.76% or 0.68%, respectively) of the supercell volume, and slightly distorts the monoclinic phase of the undoped LSO into a triclinic one with the deviations of the angles no larger than ±0.08°. Table 4 gives the selected distances for the local geometries of the Ce_{Lu1} and Ce_{Lu2} sites. Compared with the undoped system, the substitution of Ce at Lu1 site increases the distances to the six nearest oxygens by between 0.125 to 0.177 Å, while leaving the distance to the remaining (most distant) O2b atom almost unchanged. The substitution at Lu2 site increases the distances to the six coordinated oxygens by between 0.126 to 0.169 Å. The lengthening of these bonding distances is qualitatively consistent with the larger ionic radius of Ce^{3+} than that of Lu^{3+} by ~0.16 Å in the same coordination.[55] The changes of the distances to the four Si atoms in the second coordination shell upon the substitutions are in the ranges of −0.036 to 0.056 Å for Ce_{Lu1} and −0.017 to 0.090 Å for Ce_{Lu2}. The structures of the SiO_4 moieties are somewhat flexible, with slight tetrahedral deformations and the changes of Si-O distances no larger than 0.020 Å.

3.2 Electronic properties

The electronic properties of the undoped LSO were first investigated in the Lu 4*f*-core and Lu 4*f*-val schemes, to see the effects of the hybrid DFT on the calculated band gap and of the Lu $4f^{14}$ electrons on the other electronic states. Fig. 2 shows the calculated total and orbital projected densities of states (DOS) using the pure PBE and hybrid HSE06 functionals, based on the structure optimized in the Lu 4*f*-core scheme. Comparing Figs. 2(a) and 2(b), one can immediately notice that the band gap energy (E_{gap}) with HSE06 (6.35 eV) is much larger than that with PBE (4.73 eV), and is close to the experimental values of 6.4-6.8 eV as estimated from excitation and absorption spectral measurements.[9,11,56–58] On the other hand, the comparison of Figs. 2(b) and 2(c) indicates that the inclusion of the full Lu $4f^{14}$ shell as valence electrons does not substantially change the electronic properties of the other states, apart from a slight narrowing of the band gap by ~0.1 eV.

In the orbital projected DOS obtained for the undoped LSO with HSE06 (Fig. 2(b)), the O 2p states form a valence band about 6.62 eV wide just below the Fermi level (E_F), while the Lu 5*d* states mainly constitute the conduction band lying 7.35-14.01 eV above E_F. The O 2s bands lie in an energy range of 16.40-19.85 eV below E_F. There is a small peak at 6.35 eV above E_F, which constitutes the conduction band edge. This peak is mainly composed of Lu 6*s* and O 2*s* states; it has similar characteristics as Yb-trapped excitons in $SrCl_2$:Yb[59] and it might well correspond to a Lu-trapped exciton. It is noted that the orbital characters of valence and conduction bands with HSE06 are basically the same as those obtained with the pure PBE (comparing Figs. 2(a) and 2(b)), although their energy positions relative to E_F are different.

For Ce_{Lu1}- and Ce_{Lu2}-doped LSO, the total energy calculations for the two optimized structures indicate that the former substitutional doping is more favorable than the latter by 415 meV with PBE and 452 meV with HSE06. The strong tendency of Ce to occupy the Lu1 site compared to the Lu2 site is in support of the conclusions drawn from analysis of the experimental EPR spectra.[12]

In Fig. 3, we show the total and orbital-projected DOS for Ce_{Lu1}- and Ce_{Lu2}-doped LSO obtained with PBE and HSE06 in the Lu 4*f*-core scheme. One observes that the incorporation of Ce into LSO leads to formation of electronic states in the band gap, and their properties depends significantly on the choice of the XC functional. With the pure PBE functional, the Ce_{Lu1}- or Ce_{Lu2}-doped LSO are predicted to be nearly metallic with E_F positioned within the Ce 4*f* bands, see Figs. 3(a) and 3(b). With the hybrid HSE06 functional, an energy gap opens between the occupied and unoccupied Ce 4*f* states, and the two doped systems are correctly predicted to be insulating, see Figs. 3(c) and 3(d). The unoccupied 4*f* states are positioned above the bottom of the conduction band, and are broadened with respect to those with PBE due to the hybridization with the other empty states. In the DOS with both the pure and hybrid functionals, the sharp peak at the valence band edge corresponds to a lone Ce 4*f* electron, indicating a 3+ oxidation state of the Ce cation.

In Figs. 3(a)-(d), we also show the values of the computed gap (ΔE_{4f}) between the occupied Ce 4*f* band and the top of the valence band. For Ce_{Lu1}- (and Ce_{Lu2}-) doped LSO, the value of ΔE_{4f} is decreased from 4.05 eV (and 4.24 eV) with PBE to 2.81 eV (and 3.07 eV) with HSE06. Experimentally, the value of ΔE_{4f} was estimated to be about 2.6-2.9 eV[11] based on the wavelength-resolved thermally stimulated luminescence measurements. Thus, the hybrid HSE06 gives a value for ΔE_{4f} in much closer agreement with the experimental data than the standard PBE functional, especially for the more preferential Ce_{Lu1} doping. In addition, the calculated HSE06 value of ΔE_{4f} for Ce_{Lu1} is larger than that for Ce_{Lu2} (by 0.19 eV). This relative position is qualitatively consistent with the experimental results from the temperature and spectrally-resolved photoconductivity study.[60]

3.3. 4*f*→5*d* transition energies

Using the relaxed atomic structures of Ce_{Lu1}- and Ce_{Lu2}-doped LSO supercells from DFT-PBE calculations in the Lu 4*f*-core scheme, we constructed the Ce-centered embedded clusters, $(Ce_{Lu1}O_7Si_4)^{5+}$ and $(Ce_{Lu2}O_6Si_4)^{7+}$ (denoted hereafter by Ce_{Lu1} and Ce_{Lu2} for brevity), with the surroundings represented by AIMPs and point charges to account for the electrostatic, exchange, and Pauli interactions of the clusters with the embedding environments. The wavefunction-based CASSCF/CASPT2 calculations were then carried out to obtain the energy levels for Ce^{3+} $4f^1$, $5d^1$, and $6s^1$ configurations. In Table 5 we list the level energies calculated at both the spin-orbit-free and spin-orbit levels. One can see that, besides its expected importance for the $4f^1$ levels, the inclusion of the spin-orbit coupling increases the $5d^1$ and $6s^1$ level energies uniformly by around ~1000 cm^{-1} for both Ce_{Lu1} and Ce_{Lu2} clusters. A similar observation was found before for Ce^{3+} doped in $Y_3Al_5O_{12}$.[61] When comparing the calculated 4*f*→5*d* transition energies with those estimated from the experimental absorption or excitation band maxima, the calculated results for the three lowest $5d^1$ levels of Ce_{Lu1} and the two lowest $5d^1$ levels of Ce_{Lu2} agree respectively with the experimental results for Ce1 and Ce2 activation centers. The respective average deviations are 430 and 550 cm^{-1} at the spin-orbit-free level, and 610 and 1010 cm^{-1} at the spin-orbit level. For the $4f^1$, $6s^1$ and the other $5d^1$ levels, the firm experimental data are lacking and thus no comparison can be made with experiments. Table 6 lists the relative oscillator strengths computed using the CASSCF wavefunctions and CASPT2 energies for the zero-phonon transition lines from the $4f^1$ ground level ($1\Gamma_2$) to the five $5d^1$ levels ($8\text{-}12\Gamma_2$), and for Ce_{Lu1} a schematic representation is given in Fig. 4. Its intensity pattern shows a good agreement with the experimental absorption spectrum of the Ce1 center in ref. 4.

The above comparison of calculated and experimental $4f \rightarrow 5d$ transition energies provide direct evidence that the experimentally designated Ce1 and Ce2 centers are due to the Ce^{3+} ions residing in the two crystallographically inequivalent Lu sites, in support of the two-activation-model proposed by Suzuki et al..[5] Furthermore, it unambiguously identifies the Ce1 and Ce2 centers to the seven-coordinated Ce_{Lu1} and the six-coordinated Ce_{Lu2} sites, respectively. This indicates that the dopant Ce^{3+} ions preferentially occupy the larger substitutional sites, which is consistent with results of the DFT supercell total-energy calculations and also the EPR spectral measurements.[12] Along this line of thinking, the dopant Ce^{3+} is not likely to occupy the much smaller interstitial sites instead of the larger substitutional sites, before the latter are almost filled.

Table 5 also shows that, for the two lowest transitions, $4f^1\ 1\Gamma_2 \rightarrow 5d^1\ 8,9\Gamma_2$, the calculated transition energies for Ce_{Lu1} are greater than those for Ce_{Lu2} by 269 and 3648 cm^{-1}, respectively. These values are in quite good agreement with the corresponding experimental data of 931 and 3184 cm^{-1}, as estimated from the excitation or absorption band maxima. The lowering of the two transition energies from Ce_{Lu1} to Ce_{Lu2} may intuitively be explained by the increase of the crystal-field splitting of $5d^1$ levels due to a reduction of the size of the coordination polyhedron, with the average Ce-O distance decreasing from 2.463 Å in Ce_{Lu1} to 2.371 Å in Ce_{Lu2}. Considering that the change of the centroid energy might also contribute the reduction of the transition energies, in the following we will discuss the lowering of these two transition energies in a little more detail.

According to the analysis in ref. 14, each of the transition energies from the lowest $4f^1$ level ($1\Gamma_2$) to the two lowest $5d^1$ levels ($i\Gamma_2$, i = 8,9) may be decomposed into two components, i.e., the centroid-energy difference (ced) and the crystal-field stabilization (cfs) energies,

$$\Delta E(4f^1\ 1\Gamma_2 \rightarrow 5d^1\ i\Gamma_2)$$

$$= \Delta E_{ced}(4f^1 \rightarrow 5d^1) + \Delta E_{cfs}(4f^1\ 1\Gamma_2 \rightarrow 5d^1\ i\Gamma_2)$$

$$= \Delta E_{ced}(4f^1 \rightarrow 5d^1) + \Delta E_{cfs}(4f^1\ 1\Gamma_2) - \Delta E_{cfs}(5d^1\ i\Gamma_2)$$

where $\Delta E_{ced}(4f^1 \rightarrow 5d^1)$ is the centroid-energy difference between $5d^1$and $4f^1$ configurations, and $\Delta E_{cfs}(4f^1\ 1\Gamma_2)$ and $\Delta E_{cfs}(5d^1\ i\Gamma_2)$ are the crystal-field stabilization energies of the $4f^1\ 1\Gamma_2$ and $5d^1\ i\Gamma_2$ levels, relative to their respective $4f^1$ and $5d^1$ centroid energies. A schematic representation of these quantities is shown in Fig. 5, and their values for the $4f^1\ 1\Gamma_2 \rightarrow 5d^1\ i\Gamma_2$ (i = 9, 10) transitions of Ce_{Lu1} and Ce_{Lu2} are given in Table 7. From this table, we see that the centroid-energy difference, $\Delta E_{ced}(4f^1 \rightarrow 5d^1)$, shifts only by 7 cm^{-1} from Ce_{Lu1} to Ce_{Lu2}, which may be rationalized qualitatively using Judd-Morrison model.[62,63] According to this model, from Ce_{Lu1} to Ce_{Lu2}, $\Delta E_{ced}(4f^1 \rightarrow 5d^1)$ is decreased with the shortening of the average Ce-O distance, but at the same time it is increased with the decrease of the coordination number (from seven to six), and the two effects nearly cancel. Therefore, for the reduction of the $4f^1$ $1\Gamma_2 \rightarrow 5d^1$ $8,9\Gamma_2$ transition energies from Ce_{Lu1} to Ce_{Lu2}, the contribution from the change of the centroid-energy difference is negligible, and hence the contribution from the crystal-field stabilization dominates.

The crystal-field stabilization energies of the $4f^1 1\Gamma_2$ and $5d^1\ i\Gamma_2$ (i = 9, 10) levels all increase from Ce_{Lu1} to Ce_{Lu2} with the values of 236, 512, and 3891 cm^{-1}, respectively. This is consistent with the expectation that the size reduction of the coordination polyhedron from Ce_{Lu1} to Ce_{Lu2} should lead to an increased crystal-field stabilization of $4f^1$ and $5d^1$ levels. This size effect is especially pronounced for the second $5d^1\ 10\Gamma_2$ level, which leads to a reduction of the transition energy to this level by 3648 cm^{-1} from Ce_{Lu1} to Ce_{Lu2}, as compared to the value of only 269 cm^{-1} for the lowest $4f^1\ 1\Gamma_2 \rightarrow 5d^1\ 8\Gamma_2$ transition.

4. Conclusions

We have investigated the electronic properties and $4f \rightarrow 5d$ transitions of Ce-doped LSO using the hybrid DFT calculations with the periodic supercell model and the wavefunction-based CASSCF/CASPT2 calculations with the embedded cluster model, respectively. It was found that the hybrid HSE06 functional provides a Kohn-Sham band-gap value and the energy position of the occupied Ce^{3+} 4*f* states in much better agreement with experiments than the standard GGA-PBE functional. At the same time, the total energy calculations reveal that the Ce substitution into the seven-coordinated Lu1 site is strongly preferred over the six-coordinated Lu2 site, consistent with the EPR spectral observations. Based on the previously determined supercell structures, the embedded $(Ce_{Lu1}O_7Si_4)^{5+}$ and $(Ce_{Lu2}O_6Si_4)^{7+}$ clusters were constructed, with their embedding environments represented by AIMPs. The CASSCF/CASPT2 calculations with the spin-orbit coupling effects were then performed to study the $4f \rightarrow 5d$ transitions. From comparisons of the calculated and experimental transition energies, the two distinct types of $4f \rightarrow 5d$ excitation bands as observed experimentally have been identified as due to the Ce^{3+} ions located in the two substitutional Lu sites, with the experimentally designated Ce1 and Ce2 activation centers assigned to the Ce_{Lu1} and Ce_{Lu2} sites, respectively. Finally, the changes of the two lowest $4f \rightarrow 5d$ transition energies from Ce_{Lu1} to Ce_{Lu2} have been analyzed in terms of the centroid-energy difference and the crystal-field splitting.

The present study demonstrates that the DFT calculations with the screened hybrid HSE06 functional may represent an effective way in describing the position of the Ce^{3+} 4*f* states within the host band gap, which are usually difficult to obtain directly using the conventional X-ray or UV photoelectron spectroscopy due to the weakness of the 4*f* signal of the dopant ion. It also shows the ability of high-level *ab initio* calculations in elucidating the experimentally observed Ce^{3+} $4f \rightarrow 5d$ transitions, which have broad applications in the field of optical materials. A combination of the hybrid DFT supercell approach and the wavefunction-based embedded cluster method could aid in the prediction of the optical properties of Ce-doped optical materials from the minimal information of the host composition.

Acknowledgements

This work was supported by the NSFC (Grant nos 11174005, 11074315, 90922022, and 10804001), the SRF for ROCS, SEM and the program for innovative research teams in Anhui

Normal University of China. L.S. acknowledges support from MEC-Spain (Grant No. MAT2011-24586).

References

[1] G. Blasse and B. C. Grabmaier, *Luminescent Materials*, Springer-Verlag, Berlin, 1994.

[2] P. Lecoq, A. Annenkov, A. Gektin, M. Korzhik, C. Pedrini, *Inorganic Scintillators for Detector Systems: Physical Principles and Crystal Engineering* Springer-Verlag, Heidelberg, 2006.

[3] W. M. Yen, A. Shionoya, H. Yamamoto, *Phosphor Handbook* (*2nd edition*), CRC Press, Boca Raton, 2007; Chap. 4-13.

[4] C. L. Melcher, and J. S. Schweitzer, *IEEE Trans. Nucl. Sci.*, 1992, **39**, 502.

[5] H. Suzuki, T. A. Tombrello, C. L. Melcher, and J. S. Schweitzer, *Nucl. Instr. and Meth. A*, 1992, **320**, 263.

[6] H. Suzuki, and T. A. Tombrello, *IEEE Trans. Nucl. Sci.*, 1993, **40**, 380.

[7] P. Dorenbos, C. W. E. van Eijk, A. J. J. Bos, and C. L. Melcher, *J. Phys.: Condens. Matter,* 1994, **6**, 4167.

[8] J. D. Naud, T. A. Tombrello, C. L. Melcher, J. S. Schweitzer, *IEEE Trans. Nucl. Sci.*, 1996, **43**, 1324.

[9] D. W. Cooke, B. L. Bennett, K. J. McClellan, J. M. Roper, M. T. Whittaker, and A. M. Portis, *Phys. Rev. B*, 2000, **61**, 11973.

[10] G. Ren, L. Qin, S. Lu, H. Li, *Nucl. Instr. and Meth. A*, 2004, **531**, 560.

[11] A. Vedda, M. Nikl, M. Fasoli, E. Mihokova, J. Pejchal, M. Dusek, G. Ren, C. R. Stanek, K. J. McClellan, and D. D. Byler, *Phys. Rev. B*, 2008, **78**, 195123.

[12] L. Pidol, O. Guillot-Noël, A. Kahn-Harari, B. Viana, D. Pelenc, D. Gourier, *J. Phys. Chem. Solids*, 2006, **67**, 643.

[13] A. B. Muñoz-García, J. L. Pascual, Z. Barandiarán, and L. Seijo, *Phys. Rev. B*, 2010, **82**, 064114.

[14] A. B. Muñoz-García, and L. Seijo, *Phys. Rev. B*, 2010, **82**, 184118.

[15] L. Ning, F. Yang, C. Duan, Y. Zhang, J. Liang, and Z. Cui, *J. Phys.: Condens. Matter*, 2012, **24**, 055502.

[16] C. Loschen, J. Carrasco, K. M. Neyman, and F. Illas, *Phys. Rev. B*, 2007, **75**, 035115.

[17] N. Adelstein, B. S. Mun, H. L. Ray, P. N. Ross, J. B. Neaton, and L. C. De Jonghe, *Phys. Rev. B*, 2011, **83**, 205104.

[18] D. Åberg, B. Sadigh, and P. Erhart, arXiv:1201.3860v1 unpublished.

[19] V. I. Anisimov, J. Zaanen, and O. K. Andersen, *Phys. Rev. B*, 1991, **44**, 943.

[20] V. I. Anisimov, I. V. Solovyev, M. A. Korotin, M. T. Czyzyk, and G. A. Sawatzky, *Phys. Rev. B*, 1993, **48**, 16929.

[21] I. V. Solovyev, P. H. Dederichs, and V. I. Anisimov, *Phys. Rev. B*, 1994, **50** 16861.

[22] F. Wang, C. Di Valentin, and G. Pacchioni, *J. Phys. Chem. C*, 2011, **115**, 8345.

[23] A. Iwaszuk and M. Nolan, *J. Phys. Chem. C*, 2011, **115**, 12995.

[24] P. Hohenberg and W. Kohn, *Phys. Rev. B*, 1964, **136**, B864.

[25] W. Kohn and L. J. Sham, *Phys. Rev.*, 1965, **140**, A1133.

[26] J. P. Perdew, K. Burke, and M. Ernzerhof, *Phys. Rev. Lett.*, 1996, **77**, 3865.

[27] J. P. Perdew, K. Burke, and M. Ernzerhof, *Phys. Rev. Lett.*, 1997, **78**, 1396.

[28] G. Kresse and J. Furthmüller, *Phys. Rev. B*, 1996, **54**, 11169.

[29] G. Kresse and D. Joubert, *Phys. Rev. B*, 1999, **59**, 1758.

[30] P. E. Blöchl, *Phys. Rev. B*, 1994, **50**, 17953.

[31] B. G. Janesko, T. M. Henderson, G. E. Scuseria, *Phys. Chem. Chem. Phys.*, 2009, **11**, 443.

[32] T. M. Henderson, J. Paier, G. E. Scuseria, *Phys. Status Solidi B*, 2011, **248**, 767.

[33] Z. Barandiarán and L. Seijo, *J. Chem. Phys.*, 1998, **89**, 5739.

[34] A. R. Ruiz-Salvador, Z. Barandiaran, L. Seijo, unpublished.

[35] J. L. Pascual, Z. Barandiarán, and L. Seijo, *Theor. Chem. Acc.*, 2011, **129**, 545.

[36] A. Gellé and M. Lepetit, *J. Chem. Phys.*, 2008, **128**, 244716.

[37] H. M. Evjen, *Phys. Rev.*, 1932, **39**, 675.

[38] P. P. Ewald, *Ann. Phys. (Paris)*, 1921, **64**, 253.

[39] B. O. Roos, P. R. Taylor, and P. E. M. Siegbahn, *Chem. Phys.*, 1980, **48**, 157.

[40] P. E. M. Siegbahn, A. Heiberg, B. O. Roos, and B. Levy, *Phys. Scr.*, 1980, **21**, 323.

[41] P. E. M. Siegbahn, A. Heiberg, J. Almlöf, and B. O. Roos, *J. Chem. Phys.*, 1981, **74** 2384.

[42] K. Andersson, P-Å. Malmqvist, B. O. Roos, A. J. Sadlej, and K. Wolinski, *J. Phys. Chem.*, 1990, **94**, 5483.

[43] K. Andersson, P-Å. Malmqvist, B. O. Roos, *J. Chem. Phys.*, 1992, **96**, 1218.

[44] A. Zaitsevskii and J. P. Malrieu, *Chem. Phys. Lett.*, 1995, **233**, 597.

[45] J. Finley, P-Å. Malmqvist, B. O. Roos, and L. Serrano-Andrés, *Chem. Phys. Lett.*, 1998, **288**, 299.

[46] M. Douglas, N. M. Kroll, *Ann. Phys. (NY)*, 1974, **82**, 89.

[47] B. A. Hess, *Phys. Rev. A*, 1986, **33**, 3742.

[48] B. A. Hess, C. Marian, U. Wahlgren, O. Gropen, *Chem. Phys. Lett.*, 1996, **251**, 365.

[49] P-Å. Malmqvist, B. O. Roos, B. Schimmelpfennig, *Chem. Phys. Lett.*, 2002, **357**, 230.

[50] G. Karlström, R. Lindh, P-Å. Malmqvist, B. O. Roos, U. Ryde, V. Veryazov, P. O. Widmark, M. Cossi, B. Schimmelpfennig, P. Neogrady, L. Seijo, *Comput. Mater. Sci.*, 2003, **28**, 22.

[51] L. Seijo, Z. Barandiarán, and B. Ordejón, *Mol. Phys.*, 2003, **101**, 73.

[52] Z. Barandiaran and L. Seijo, *Can. J. Chem.*, 1992, **70**, 409.

[53] T. Gustafsson, M. Klintenberg, S. E. Derenzo, M. J. Weber, and J. O. Thomas, *Acta Cryst. C*, 2001, **57,** 668.

[54] L. Ning, Y. Zhang, Z. Cui, *J. Phys. Condens. Matter*, 2009, **21**, 455601.

[55] R. D. Shannon, *Acta Cryst. A*, 1976, **32**, 751.

[56] M. Kobayashi, M. Ishii, and C. L. Melcher, *Nucl. Instr. and Meth. A*, 1993, **335**, 509.

[57] I. A. Kamenskikha, V. V. Mikhailina, I. H. Munrob, D. Y. Petrovykha, D. A. Shawb, P. A. Studenikinc, A. N. Vasil'eva, I. A. Zagumennyic, andYu. D. Zavartsevc, *Radiat. Eff. Defect S.*, 1995, **135,** 391.

[58] A. Lempicki, J. Glodo, *Nucl. Instr. and Meth. A*, 1998, **416**, 333.

[59] G. Sánchez-Sanz, L. Seijo, and Z. Barandiarán, *J. Chem. Phys.*, 2010, **133**, 114509.

[60] E. van der Kolk, S. A. Basun, G. F. Imbusch, and W. M. Yen, *Appl. Phys. Lett.*, 2003, **83**, 1740.

[61] J. Gracia, L. Seijo, Z. Barandiarán, D. Curulla, H. Niemansverdriet, and W. van Gennip, *J. Lumin.*, 2008, **128**, 1248.

[62] B. R. Judd, *Phys. Rev. Lett.*, 1977, **39**, 242.

[63] C. A. Morrison, *J. Chem. Phys.*, 1980, **72**, 1001.

Table 1 Calculated and experimental lattice parameters for the LSO crystal.

Method	Reference	*a* (Å)	*b* (Å)	*c* (Å)	*β* (deg)
DFT-PBE (Lu 4*f*-core)	This work	14.282	6.669	10.284	122.019
DFT-PBE (Lu 4*f*-val)	This work	14.384	6.725	10.380	122.079
Experiment	ref. 53	14.277	6.640	10.247	122.224

Table 2 Calculated internal parameters for the LSO crystal. The experimental (Expt.) data from ref. 53 are also listed for comparison.

	Method	*x*	*y*	*z*		Method	*x*	*y*	*z*
Lu1	Lu 4*f*-core	0.5382	0.7567	0.4711	O2	Lu 4*f*-core	0.3782	0.7885	0.1698
	Lu 4*f*-val	0.5383	0.7564	0.4705		Lu 4*f*-val	0.3780	0.7867	0.1705
	Expt.	0.5373	0.7559	0.4671		Expt.	0.3802	0.7883	0.1762
Lu2	Lu 4*f*-core	0.1411	0.3806	−0.1612	O3	Lu 4*f*-core	0.2010	0.6508	0.1783
	Lu 4*f*-val	0.1417	0.3816	−0.1614		Lu 4*f*-val	0.2020	0.6508	0.1786
	Expt.	0.1409	0.3774	−0.1636		Expt.	0.2023	0.6490	0.1768
Si	Lu 4*f*-core	0.3175	0.5921	0.1936	O4	Lu 4*f*-core	0.2972	0.4234	0.0654
	Lu 4*f*-val	0.3177	0.5919	0.1942		Lu 4*f*-val	0.2973	0.4245	0.0668
	Expt.	0.3179	0.5917	0.1931		Expt.	0.2984	0.4289	0.0630
O1	Lu 4*f*-core	0.4120	0.5130	0.3655	O5	Lu 4*f*-core	0.0166	0.4042	−0.1040
	Lu 4*f*-val	0.4112	0.5129	0.3647		Lu 4*f*-val	0.0167	0.4054	−0.1039
	Expt.	0.4112	0.5062	0.3620		Expt.	0.0177	0.4034	−0.1025

Table 3 Calculated lattice parameters and volumes for the Ce_{Lu1}- and Ce_{Lu2}-doped LSO (1 × 2 × 1) supercells. The percent changes in parentheses were taken with respect to the volume of the undoped LSO.

	LSO	LSO:Ce_{Lu1}	LSO:Ce_{Lu2}
a (Å)	14.282	14.285	14.292
$2b$ (Å)	13.337	13.364	13.375
c (Å)	10.284	10.331	10.311
α (deg)	90.000	90.047	89.945
β (deg)	122.019	121.940	121.961
γ (deg)	90.000	89.852	89.878
Volume (Å^3)	1660.991	1673.609 (+0.76%)	1672.296 (+0.68%)

Table 4 Calculated distances (in Å) from the dopant site to the atoms in the first and second coordination shells before and after the Ce_{Lu1} and Ce_{Lu2} substitutions in LSO. The values in parentheses are the differences taken with respect to the data before substitution. See Fig.1 for the definition of atomic labels.

	LSO M = Lu1	LSO:Ce_{Lu1} M = Ce_{Lu1}		LSO M = Lu2	LSO:Ce_{Lu2} M = Ce_{Lu2}
M−O1a	2.235	2.378 (+0.143)	M−O2	2.226	2.376 (+0.150)
O1b	2.302	2.426 (+0.125)	O3	2.234	2.376 (+0.142)
O2a	2.325	2.489 (+0.164)	O4a	2.215	2.384 (+0.169)
O2b	2.713	2.710 (−0.003)	O4b	2.230	2.389 (+0.159)
O3	2.254	2.412 (+0.159)	O5a	2.154	2.281 (+0.126)
O5a	2.141	2.296 (+0.154)	O5b	2.271	2.424 (+0.152)
O5b	2.353	2.530 (+0.177)			
M−Si1	3.122	3.169 (+0.047)	M−Si1	3.262	3.245 (−0.017)
Si2	3.468	3.432 (−0.036)	Si2	3.547	3.585 (+0.038)
Si3	3.532	3.582 (+0.049)	Si3	3.606	3.695 (+0.090)
Si4	3.743	3.799 (+0.056)	Si4	3.451	3.523 (+0.072)

Table 5 Calculated energy levels of the $4f^1$, $5d^1$, and $6s^1$ configurations for the $(Ce_{Lu1}O_7Si_4)^{5+}$ and $(Ce_{Lu2}O_6Si_4)^{7+}$ clusters embedded in LSO. The experimental data were taken from the average of the excitation and absorption peak energies in refs. 4,6,7,9 and 10 for Ce1 center and refs. 4 and 6 for Ce2 center. All values are in units of cm^{-1}.

	Calculation without spin-orbit coupling			Calculation with spin-orbit coupling			Experiments	
		Ce_{Lu1}	Ce_{Lu2}		Ce_{Lu1}	Ce_{Lu2}	Ce1	Ce2
$4f^1$ levels	1^2A	0	0	$1\Gamma_2$	0	0		
	2^2A	282	149	$2\Gamma_2$	373	430		
	3^2A	369	379	$3\Gamma_2$	676	1116		
	4^2A	466	541	$4\Gamma_2$	2227	2173		
	5^2A	534	1050	$5\Gamma_2$	2447	2648		
	6^2A	869	1738	$6\Gamma_2$	2742	3252		
	7^2A	1849	2349	$7\Gamma_2$	3480	3978		
$5d^1$ levels	8^2A	27908	27748	$8\Gamma_2$	28872	28603	28070	27139
	9^2A	33905	30208	$9\Gamma_2$	34905	31257	33884	30700
	10^2A	36945	32376	$10\Gamma_2$	38027	33518	38017	
	11^2A	46604	50846	$11\Gamma_2$	47812	51966		
	12^2A	51433	56967	$12\Gamma_2$	52592	58082		
$6s^1$ level	13^2A	72192	72188	$13\Gamma_2$	73277	73248		

Table 6 Computed relative oscillator strengths of 4*f* →5*d* transitions of Ce_{Lu1} and Ce_{Lu2} in LSO at the spin-orbit level.

	Ce_{Lu1}		Ce_{Lu2}	
	Transition energy	Relative oscillator strength	Transition energy	Relative oscillator strength
$4f^1\ 1\Gamma_2 \rightarrow 5d^1\ 8\Gamma_2$	28872	1.00	28603	0.93
$9\Gamma_2$	34905	0.45	31257	0.58
$10\Gamma_2$	38027	0.40	33518	0.25
$11\Gamma_2$	47812	0.14	51966	0.31
$12\Gamma_2$	52592	0.36	58082	0.18

Table 7 Analysis of the shifts of the two lowest 4*f*→5*d* transition energies from Ce_{Lu1} to Ce_{Lu2} in LSO in terms of the changes of the centroid-energy difference (ced) and the crystal-field stabilization (cfs) energy. All numbers are in units of cm^{-1}.

	Ce_{Lu1}	Ce_{Lu2}	Shift from Ce_{Lu1} to Ce_{Lu2}
$\Delta E_{ce}(4f^1)$	1706	1942	236
$\Delta E_{ce}(5d^1)$	40442	40685	243
$\Delta E_{ced}\ (4f^1 \rightarrow 5d^1)$	38736	38743	7
$\Delta E_{cfs}(4f^1\ 1\Gamma_2)$	1706	1942	236
$\Delta E_{cfs}\ (5d^1\ 8\Gamma_2)$	11570	12082	512
$\Delta E_{cfs}\ (5d^1\ 9\Gamma_2)$	5537	9428	3891
$\Delta E_{cfs}\ (4f^1\ 1\Gamma_2 \rightarrow 5d^1\ 8\Gamma_2)$	−9864	−10140	−276
$\rightarrow 5d^1\ 9\Gamma_2)$	−3831	−7486	−3655
$\Delta E\ (4f^1\ 1\Gamma_2 \rightarrow 5d^1\ 8\Gamma_2)$	28872	26110	−269
$\rightarrow 5d^1\ 9\Gamma_2)$	34905	30503	−3648

Figure captions

Fig. 1 Schematic representations of the local coordination structures of Ce^{3+} at the two lutetium (Lu1 and Lu2) sites in LSO. The numerical labels on oxygen atoms specify the crystallographic types, with "a" and "b" used to characterize the atoms of the same type. The labels on silicon are only for differentiation of the atoms.

Fig. 2 Total and orbital-projected DOS for the LSO crystal calculated using DFT with the PBE and HSE06 functionals. The labels "Lu 4*f*-core" and "Lu 4*f*-val" denote the calculations with the Lu $4f^{14}$ electrons treated as core and valence electrons respectively, and the DOS for the Lu 4*f* states in (c) are shaded in light gray. The derived band-gap energies (E_{gap}) are indicated in the legends. The Fermi energy is set as zero energy.

Fig. 3 Total and orbital-projected DOS for the Ce_{Lu1}- and Ce_{Lu2}-doped LSO crystals obtained using DFT with the PBE and HSE06 functionals in the Lu 4*f*-core scheme. The energies of the gaps (ΔE_{4f}) between the occupied Ce^{3+} 4*f* bands and the tops of O 2p valence bands are shown in the legends. The DOS for the Ce^{3+} 4*f* states have been enlarged by a factor of two, and are shaded in light gray. The Fermi energies are indicated by the dashed lines.

Fig. 4 Schematic diagram for the calculated energies and relative oscillator strengths of the $4f \rightarrow 5d$ transitions in Ce_{Lu1}-doped LSO. The inset shows the experimental absorption spectrum adapted from ref. 4 for comparison.

Fig. 5 Schematic representation for the energy levels of the $4f^1$ and $5d^1$ configurations of Ce^{3+} in LSO. ΔE_{ced} denotes the centroid-energy difference between the two configurations, and ΔE_{cfs} the crystal-field stabilization energy of the levels.

FIG. 1

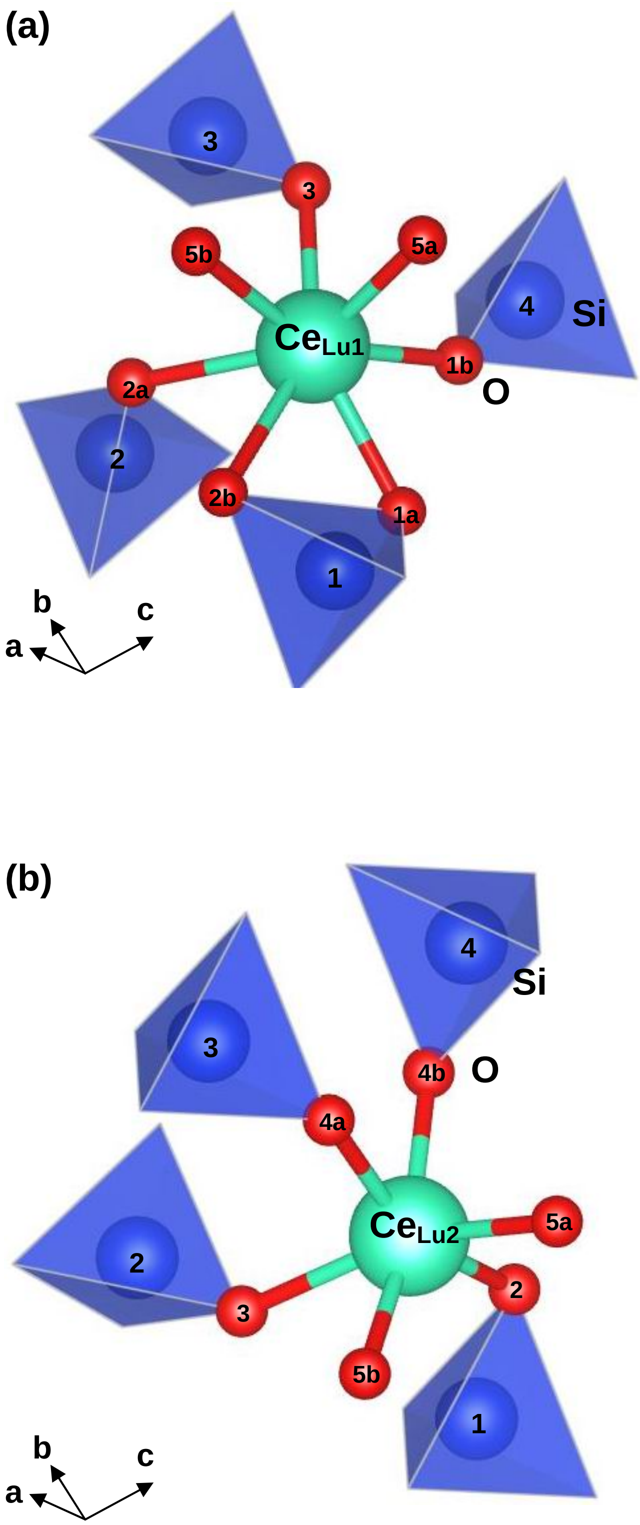
(a)
3
3
5b
5a
4
Si
Ce_{Lu1}
1b
O
2a
2
2b
1a
1
b
c
a
(b)
4
Si
3
4b
O
4a
2
Ce_{Lu2}
5a
3
2
5b
1
b
c
a

FIG. 2

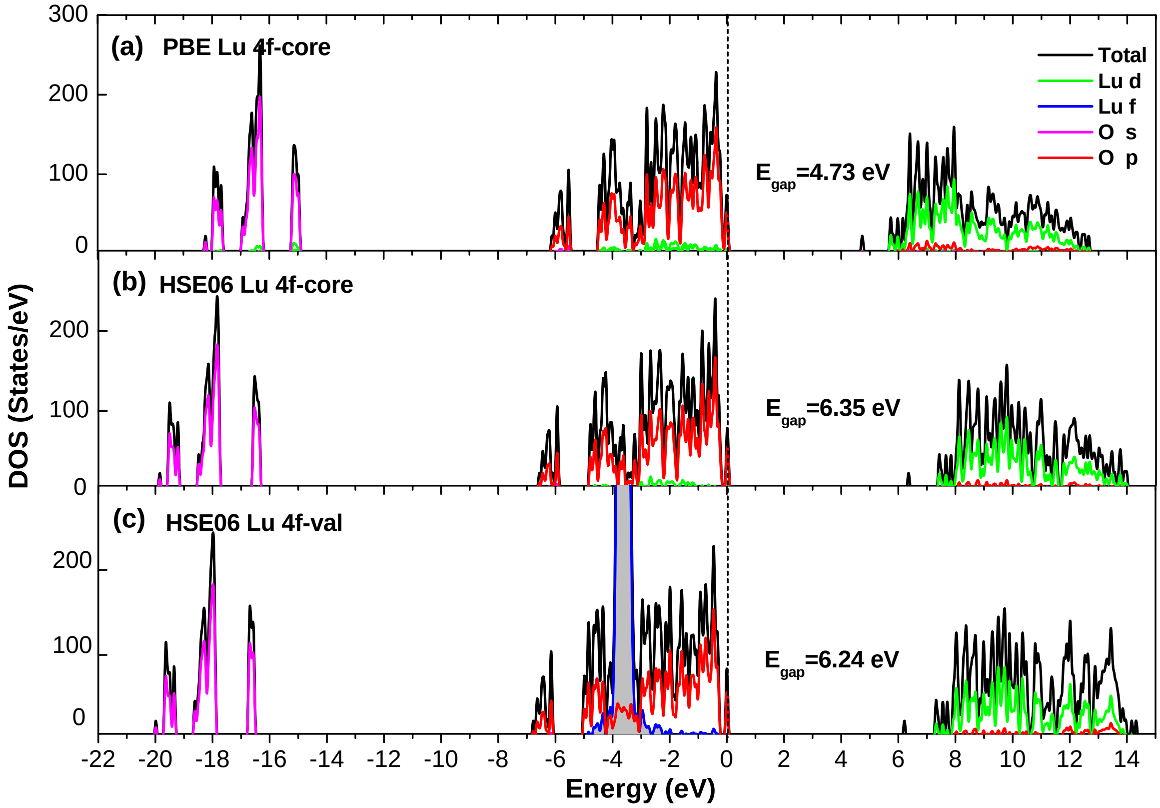

(a) PBE Lu 4f-core
(b) HSE06 Lu 4f-core
(c) HSE06 Lu 4f-val
Total
Lu d
Lu f
O s
O p
E$_{gap}$=4.73 eV
E$_{gap}$=6.35 eV
E$_{gap}$=6.24 eV
DOS (States/eV)
Energy (eV)

FIG. 3

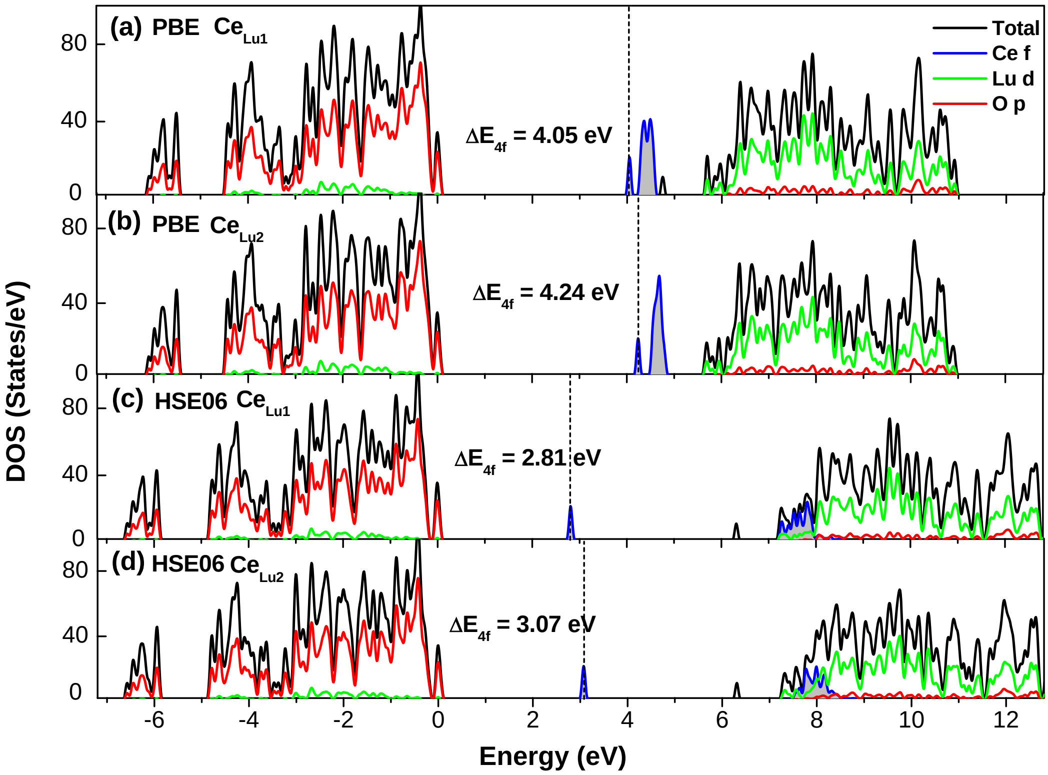

(a) PBE Ce_{Lu1}
(b) PBE Ce_{Lu2}
(c) HSE06 Ce_{Lu1}
(d) HSE06 Ce_{Lu2}
ΔE_{4f} = 4.05 eV
ΔE_{4f} = 4.24 eV
ΔE_{4f} = 2.81 eV
ΔE_{4f} = 3.07 eV
Total
Ce f
Lu d
O p
DOS (States/eV)
Energy (eV)
0
40
80
-6
-4
-2
0
2
4
6
8
10
12

FIG. 4

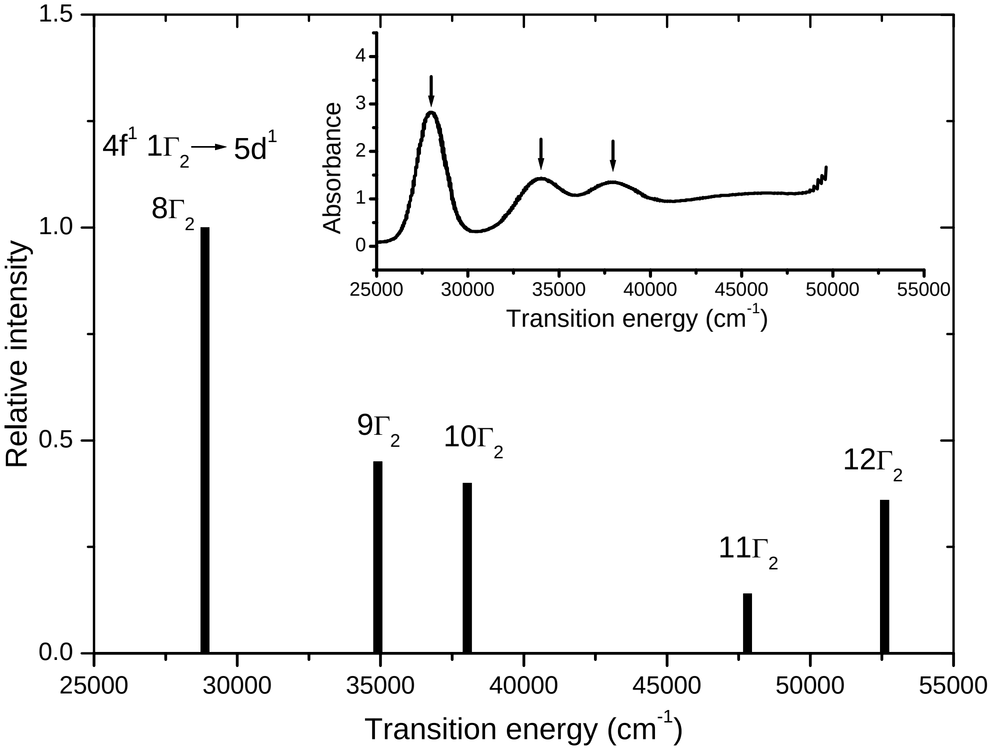

1.5
1.0
0.5
0.0
Relative intensity
25000
30000
35000
40000
45000
50000
55000
Transition energy (cm-1)
4f1 1Γ2 → 5d1
8Γ2
9Γ2
10Γ2
11Γ2
12Γ2
Absorbance
4
3
2
1
0

FIG. 5

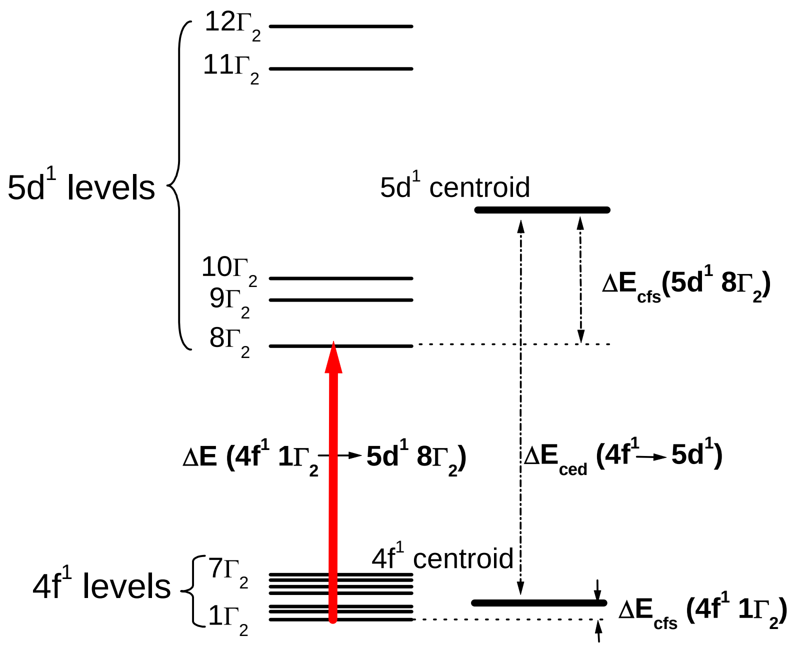

12Γ2
11Γ2
5d1 levels
5d1 centroid
10Γ2
9Γ2
8Γ2
ΔEcfs(5d1 8Γ2)
ΔE (4f1 1Γ2→5d1 8Γ2)
ΔEced (4f1→5d1)
4f1 centroid
7Γ2
4f1 levels
1Γ2
ΔEcfs (4f1 1Γ2)